Current Optics and Photonics
Vol. 3, No. 3, June 2019, pp. 248-255

ISSN: 2508-7266(Print) / ISSN: 2508-7274(Online)
DOI: https://doi.org/10.3807/COPP.2019.3.3.248

Up-conversion Luminescence Characterization of CeO_2:Ho^{3+}/Yb^{3+} Particles Prepared by Spray Pyrolysis

Kyeong Youl Jung[1]*, Byeong Ho Min[1], Dae Sung Kim[2], and Byung-Ki Choi[3]

[1]Department of Chemical Engineering, Kongju National University, Cheonan 31080, Korea
[2]Eco-composite Materials Center, Korea Institute of Ceramic Engineering & Technology (KICET), Jinju 52851, Korea
[3]CQV Co., Ltd., Jinchen 27845, Korea

(Received January 26, 2019 : revised February 25, 2019 : accepted February 28, 2019)

Spherical CeO_2:Ho^{3+}/Yb^{3+} particles were synthesized using spray pyrolysis, and the upconversion (UC) properties were investigated with changing the preparation conditions and the infrared pumping power. The resulting particles had a size of about 1 μm and hollow structure. The prepared CeO_2:Ho^{3+}/Yb^{3+} particles exhibited intense green emission due to the $^5F_4/^5S_2 \rightarrow {}^5I_8$ transition of Ho^{3+} and showed weak red or near-IR peaks. In terms of achieving the highest UC emission, the optimal concentrations of Ho^{3+} and Yb^{3+} were 0.3% and 2.0%, respectively. The UC emission intensity of prepared CeO_2:Ho^{3+}/Yb^{3+} particles had a linear relationship with crystallite size and concentration quenching was caused by dipole-dipole interaction between the same ions. Based on the dependency of UC emission on the pumping power, the observed green upconversion was achieved through a typical two-photon process and concluded that the main energy transfer from Yb^{3+} to Ho^{3+} was involved in the ground-state adsorption (GSA) process.

Keywords : Spray pyrolysis, Phosphor, Upconversion, Energy transfer
OCIS codes : (160.2540) Fluorescent and luminescent materials; (160.5690) Rare-earth-doped materials; (160.4760) Optical properties

I. INTRODUCTION

As the global market grows rapidly, forgery of products or intellectual property becomes a big problem. Companies are trying to protect their products from counterfeiting. As a result, it is very important for a company to develop its own anticounterfeiting technology. Upconversion (UC) phosphors, which convert near-infrared (NIR) to visible light, have attracted considerable attention as potential security materials because they can easily distinguish counterfeit products from original products using self-emission under NIR illumination [1-5]. The state of the art on UC phosphor technology is well introduced in recent literature [6, 7]. Most UC materials contain lanthanide ions (Ln^{3+}) as activators and sensitizers. These lanthanide ions are incorporated into inorganic hosts and play a key role in determining the luminescence color and efficiency. The composition of host materials also directly affects the UC emission color or efficiency even if the activator and sensitizer ions are same. Thus, many efforts have been dedicated to find novel hosts with the intention of achieving an improved UC performance [8-11].

Lanthanide ions such as Er^{3+}, Ho^{3+}, Tm^{3+} and Yb^{3+} have been used as the dopants for UC materials. Yb^{3+} is an excellent sensitizer because it has a large absorption cross-section at 980 nm compared with other Ln^{3+} ions (Ln^{3+} = Er^{3+}, Ho^{3+} and Tm^{3+}) [12]. Therefore, ion pairs such as Er^{3+}/Yb^{3+}, Ho^{3+}/Yb^{3+} and Tm^{3+}/Yb^{3+} are used to improve the UC luminescence. Host materials for UC phosphors are required to have high transparency, good optical or chemical stability and low phonon energy [6]. Given this, CeO_2 is a good host because it has high transparency in the visible region, excellent chemical stability, and low photon

*Corresponding author: kyjung@kongju.ac.kr, ORCID 0000-0002-9550-9285
Color versions of one or more of the figures in this paper are available online.

energy (~470 cm^{-1}) [13]. Thus, ceria has been used in a number of research fields including catalysts, phosphors, and sensors [14-16]. Also, lanthanide ion radii are close to the ionic radius of Ce^{4+} so that the dopants can be easily substituted into the lattice of CeO_2. There are a number of studies that have focused on Er^{3+} or Er^{3+}/Yb^{3+}-doped CeO_2 characteristics [13, 17-19]. $CeO_2:Er^{3+}/Yb^{3+}$ has both green and red UC emissions, and the emission ratio of green to red is controllable by changing the concentration of Yb^{3+}. Similarly to the Er^{3+}/Yb^{3+} couple, Ho^{3+}/Yb^{3+} couples can also generate green or red depending on the type of host material. Referring to the previous studies including Y_2O_3 [20-22] and Gd_2O_3 [23, 24], using a Ho^{3+}/Yb^{3+} pair rather than an Er^{3+}/Yb^{3+} ion pair can be more beneficial for implementing high intense green UC phosphors. Nevertheless, there are not much studies on the synthesis and UC characteristics of $CeO_2:Ho^{3+}/Yb^{3+}$ compared with $CeO_2:Er^{3+}/Yb^{3+}$. In 2010, for the first time, Babu *et al.* reported the green emission of $CeO_2:Ho^{3+}/Yb^{3+}$ and applied it to bio-imaging and therapeutics [25]. Avram *et al.* investigated the dependence of the UC emission color of $CeO_2:Ho^{3+}/Yb^{3+}$ on the excitation wavelength, and they observed the tunable ratio of red to green while increasing the powder density of an ac laser diode at 980 nm [26].

Although host and activator are the same, the luminescence properties of phosphor particles depend on their size and distribution, morphology, activator concentration, and activator distribution within hosts. To achieve good performance in various application fields, phosphor particles are needed to have fine size (about 1 μm) and spherical morphology. Also, high phase purity or uniform distribution of activators is critical to achieve high luminescence. Therefore, it is important to develop a synthesis method that can produce phosphor with excellent optical and morphological properties. Spray pyrolysis has been applied to prepare various functional materials [27-30]. One particle comes from one droplet in the spray pyrolysis. All elements consisting of phosphor can exist a homogeneously mixed state in the produced particle in a molecular level as long as no phase separation occurs during the drying step. Consequently, the spray pyrolysis can easily produce fine-sized spherical particles having homogeneous distribution of activators within host particles. Therefore, spray pyrolysis is a good synthesis method that can prepare multi-component phosphors such as $BaMgAl_{10}O_{17}$:Eu, $Y_3Al_5O_{12}$:Ce and (Y, Ln)VO_4:Eu into spherical shape and fine size [31-33]. Nevertheless, to our best knowledge, there is no report on the synthesis of $CeO_2:Ho^{3+}/Yb^{3+}$ using the spray pyrolysis process. In this work, the spray pyrolysis was applied to prepare $CeO_2:Ho^{3+}/Yb^{3+}$ having high UC emission to be identified by the naked eye. To do this, the UC properties were optimized by controlling the Ho^{3+} and Yb^{3+} concentration. The crystallinity of $CeO_2:Ho^{3+}/Yb^{3+}$ was controlled by changing the calcination temperature from 900°C to 1200°C in order to find the relationship with the UC intensity. Finally, the UC mechanism of $CeO_2:Ho^{3+}/Yb^{3+}$ prepared by spray pyrolysis was investigated by monitoring the dependency of the UC intensity on the IR pumping power while changing the activator concentration.

II. EXPERIMENTAL

The $CeO_2:Ho^{3+}/Yb^{3+}$ particles were synthesized by a spray pyrolysis process consisting of an ultrasonic nebulizer (1.7 MHz), a quartz tube (ID = 55 mm and length = 1200 mm), an electrical furnace and a Teflon bag filter. Cerium nitrate hexahydrate (Aldrich, 99.99%), holmium oxide (Aldrich, 99.9%) and ytterbium oxide (Aldrich, 99.99%) were used as the starting materials. Spray solution was prepared by the following procedure. The activator (Ho^{3+}) and sensitizer (Yb^{3+}) precursors were dissolved by using nitric acid as a nitrate form and followed by adding the purified water until the total solution becomes 250 mL. Cerium nitrate was dissolved in 250 mL of purified water and mixed with the activator and sensitizer solution. The total salt concentration was kept at 0.2 M. The Ho (x) and Yb (y) contents in $Ce_{1-x-y}O_2:Ho_x/Yb_y$ were changed from $x = 0.001$ to $x = 0.007$ and from $y = 0.005$ to $y = 0.060$. The prepared precursor solution was turned into droplets using an ultrasonic nebulizer and carried into the quartz reactor (900°C) by air (30 L/min). The produced particles were collected by a Teflon bag filter and calcined at the temperature range from 900 to 1200°C for 3 h in an air environment.

The UC emission of all samples was measured using a spectrophotometer (PerkinElmer, LS 50) under the excitation of 980 nm IR laser (Optoenergy, PL980P330J). The dependency of UC emission on the pumping powder was monitored by varying the pumping power from 100 to 1000 mW. The crystal phase of $CeO_2:Ho^{3+}/Yb^{3+}$ powder prepared was identified by X-ray diffraction (XRD, Rigaku, MiniFlex600) measurement. The morphology of the prepared particles were identified by using high-resolution scanning electron microscopy (HR-SEM, Hitachi S4800) at the Korea Basic Science Institute (KBSI).

III. RESULTS AND DISCUSSION

Figure 1 shows the UC emission spectrum and energy level diagram of $CeO_2:Ho^{3+}$ ($x = 0.005$) and $CeO_2:Ho^{3+}/Yb^{3+}$ ($x = 0.005$, $y = 0.005$) particles prepared by spray pyrolysis and calcined at 1000°C. The observed three peaks are due to the $^5F_4/^5S_2 \rightarrow {}^5I_8$ (550 nm, green), $^5F_5 \rightarrow {}^5I_8$ (670 nm, red) and $^5F_4/^5S_2 \rightarrow {}^5I_7$ (760 nm, NIR) transition of Ho^{3+} ions [26]. Figure 1(b) shows the energy level diagram of Ho^{3+} and Yb^{3+}. The absorption cross section of Yb^{3+} ions is much larger than that of Ho^{3+} ions. Thus, the Yb^{3+} ions absorbs much more photons than the Ho^{3+} ions. The $^2F_{5/2}$ energy level of Yb^{3+} is located slightly higher than the $^5I_6$

level of Ho^{3+}. Thus, the energy transfer (ET) from Yb^{3+} to Ho^{3+} is possible and can take part in both ground state adsorption (GSA) and excited state adsorption (ESA) processes. The photons populated in the $^5I_6$ state of Ho^{3+} through the GSA process can be further excited to the $^5F_4/^5S_2$ level via the ESA or ET processes. The photons excited to the $^5F_4/^5S_2$ level decay to the $^5I_8$ and $^5I_7$ states of Ho^{3+}, emitting green and NIR light, respectively. A part of photons in the $^5F_4/^5S_2$ level can also relax nonradiatively to the $^5F_5$ level and radiatively to the ground state ($^5I_8$), which corresponds to the red emission at about 670 nm. The red emission can be also possible through the consecutive path of GSA ($^5I_8 \rightarrow {}^5I_6$), non-radiative relaxation ($^5I_6 \rightarrow {}^5I_7$), ESA ($^5I_7 \rightarrow {}^5F_5$) and radiative decay ($^5F_5 \rightarrow {}^5I_8$). For CeO_2:Ho^{3+}, as shown in Fig. 1(a), the green emission is strong, but other two (red and NIR) peaks are weak. That is, the UC emission of CeO_2:Ho^{3+} is achieved mainly through the $^5F_4/^5S_2 \rightarrow {}^5I_8$ transition after the ground-state absorption (GSA) ($^5I_8 \rightarrow {}^5I_6$) and excitation-state absorption (ESA) ($^5I_6 \rightarrow {}^5F_4$). The UC emission of CeO_2:Ho^{3+}/Yb^{3+} is much higher than that of CeO_2:Ho^{3+}. Given this, the Yb^{3+} co-doping leads to the enhanced UC intensity due to an

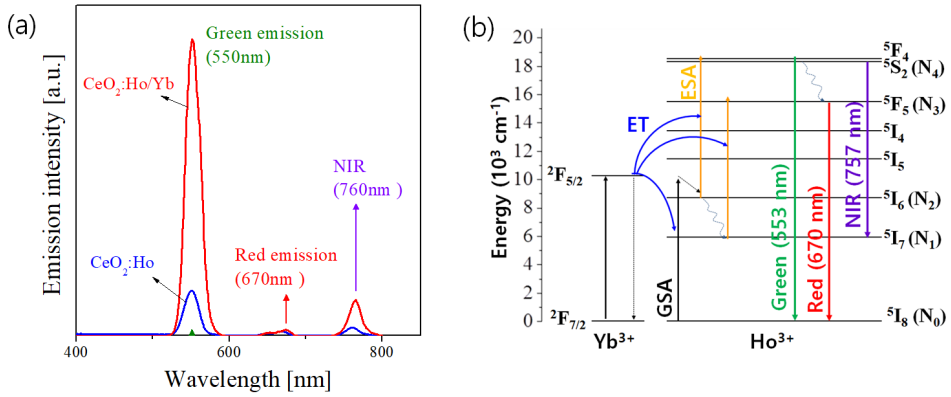

FIG. 1. (a) Emission spectra measured under the excitation of 980 nm IR laser for CeO_2:Ho^{3+} and CeO_2:Ho^{3+}/Yb^{3+} particles prepared by spray pyrolysis and (b) energy-level diagram for Ho^{3+} and Yb^{3+} ions.

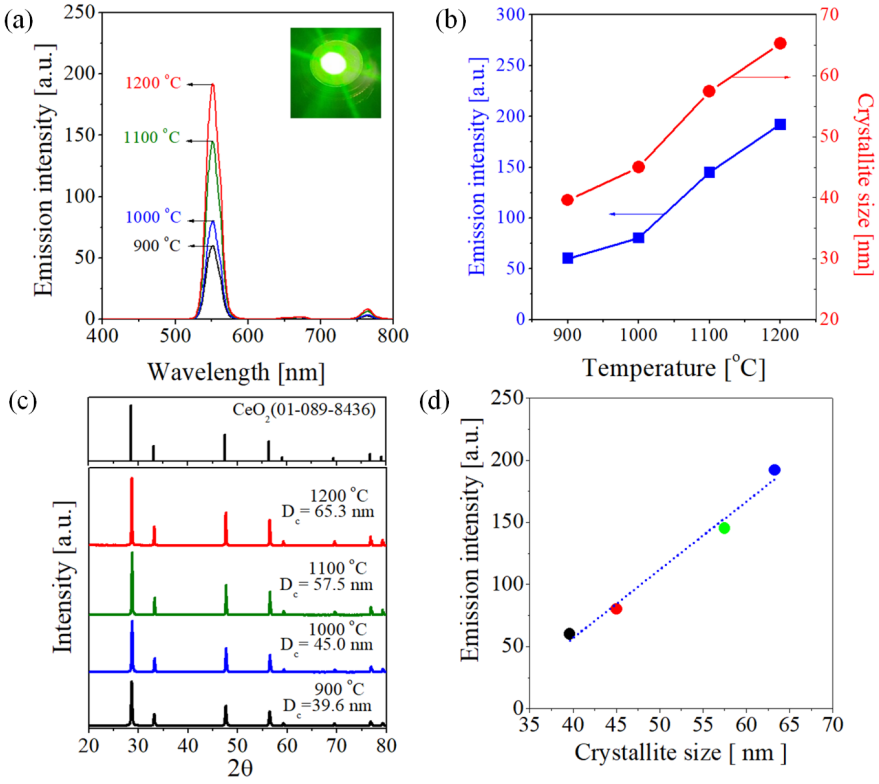

FIG. 2. (a) Emission spectra and (b) emission intensity as a function of calcination temperature, (c) XRD patterns, and (d) emission intensity as a function of crystallite size for CeO_2:Ho^{3+}/Yb^{3+} powder prepared by spray pyrolysis.

effective energy transfer from Yb^{3+} to Ho^{3+}.

The UC properties of CeO_2:Ho^{3+}/Yb^{3+} prepared by spray pyrolysis were investigated by changing the calcination temperature. Figure 2(a) shows the UC spectra of CeO_2:Ho^{3+}/Yb^{3+} particles and the green emission intensity at 550 nm is shown in Fig. 2(b) as a function of the calcination temperature. There is no difference in the emission spectrum except the intensity with changing the calcination temperature, indicating that the main UC path of CeO_2:Ho^{3+}/Yb^{3+} is not affected. The UC emission of the CeO_2:Ho^{3+}/Yb^{3+} sample calcined at 1200°C was photographed under irradiation of 980 nm IR. As shown in the inset of Fig. 1(a). The CeO_2:Ho^{3+}/Yb^{3+} particles have excellent green emission. The emission intensity increases gradually as the calcination temperature increases, which is mainly due to the increase of crystallinity. To confirm this, XRD measurements were carried out. Figure 2(c) shows XRD patterns of the prepared CeO_2:Ho^{3+}/Yb^{3+} samples. All peaks are in good agreement with the cubic phase of CeO_2 and no impurity phase is observed regardless of the calcination temperature. For solid oxides, the crystallinity can be evaluated from the crystallite size. That is, the larger the crystallite size, the higher the crystallinity. The crystallite size was calculated by Scherrer's equation, and the resulting values are shown within Fig. 2(c). The crystallite size increases as the calcination temperature increases, indicating that the crystallinity is gradually improved. Figure 2(d) shows the dependence of the emission intensity on the crystallite size. The emission intensity has a linear relation with the crystallite size. This result supports that the enhancement in the crystallinity is critical to improve the emission intensity.

Figure 3 is SEM photos of CeO_2:Ho^{3+}/Yb^{3+} particles prepared by changing the calcination temperature from 900 to 1200°C. The formation mechanism of CeO_2:Ho/Yb hollow particles in spray pyrolysis is also shown in Fig. 3(f). The as-prepared particles have spherical shape that is maintained even after the calcination at 1200°C. The prepared particles show a hollow structure that is frequently encountered in a conventional spray pyrolysis process. No significant change in the particle morphology was observed by increasing the calcination temperature. As shown in Fig. 3(f), the spray pyrolysis produces particles through drying, precipitation and pyrolysis (thermal decomposition). The fast drying of droplets increases the surface concentration of droplets. As a result, the salt concentration on the surface of the water droplet reaches the supersaturation point, so surface precipitation occurs and forms a shell layer. Thereafter, as the water drying progresses further, the precipitation proceeds on the inner surface of the initially formed solid shell. In this step, evaporated water molecules escape solid layers, making the precipitated layer porous. Next, thermal decomposition (pyrolysis) takes place, producing many gas molecules. Because the solid layer is porous, these gas molecules can be ejected outside the solid layer without the deformation of the particle. Finally, the shell layer is turned into nano-sized crystals by the high-temperature

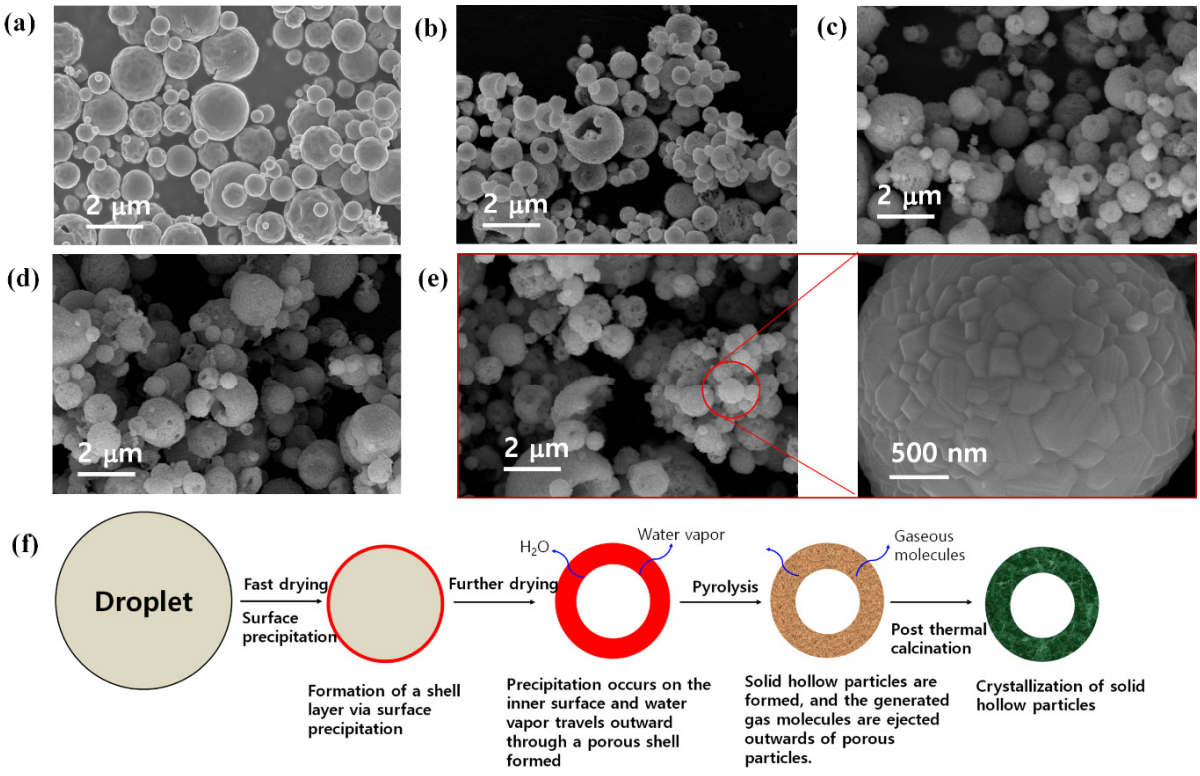

FIG. 3. SEM photos of CeO_2:Ho^{3+}/Yb^{3+} powder prepared by spray pyrolysis: (a) as-prepared, (b) 900°C, (c) 1000°C, (d) 1100°C and (e) 1200°C. (f) Particle formation mechanism in spray pyrolysis.

calcination, which can be identified in Fig. 3(e). The obtained CeO_2:Ho^{3+}/Yb^{3+} particles are about 1 μm in size and have a hollow structure. Based on the SEM result, it was confirmed that spherical and fine-sized CeO_2:Ho^{3+}/Yb^{3+} particles with high green UC emission could be synthesized by spray pyrolysis.

Figure 4 shows the effect of the Ho^{3+} and Yb^{3+} content on the UC properties of CeO_2:Ho^{3+}/Yb^{3+} particles prepared by spray pyrolysis. First, at the fixed Ho^{3+} content (x = 0.005) the UC emission is monitored by changing the Yb^{3+} content (y) from 0.005 to 0.06 and the resulting spectra are shown in Fig. 4(a). The UC intensity was significantly improved by the introduction of Yb^{3+}, and the highest emission intensity was observed at y = 0.02. There was no significant improvement in the red or NIR emission. Next, the UC emission is examined by changing the Ho^{3+} content (x) at y = 0.02 and the resulting spectra are shown in Fig. 4(b). The highest UC emission was obtained at x = 0.003. Figure 4(c) shows the effect of both Ho^{3+} and Yb^{3+} contents on the UC emission intensity (λ_{em} = 553 nm). From these results, the optimum contents of Ho^{3+} (x) and Yb^{3+} (y) to achieve the highest UC intensity were determined as x = 0.003 and y = 0.02.

The luminescence intensity of CeO_2:Ho^{3+}/Yb^{3+} is reduced when the Ho^{3+} content is larger than 0.003 and the Yb^{3+} content is larger than 0.02. The concentration quenching of the emission intensity in phosphor materials is basically connected with the non-radiative energy transfer between dopants. The critical distance (R_c) between dopants for the non-radiative energy transfer can be calculated by the following equation [34].

$$R_c = 2\left(\frac{3V}{4\pi N z_c}\right)^{1/3} \quad (1)$$

where z_c is the critical concentration, V is the unit cell volume (158.5 Å) and N is the number of cations in the unit cell (N = 4). Then, the calculated critical distances are about 15.6 Å and 29.3 Å for Yb^{3+} (z_c = 0.02) and Ho^{3+} (z_c = 0.003), respectively. Also, the average critical distance for the total dopants (z_c = 0.023) is about 14.9 Å. The exchange interaction is known to be possible when the critical distance is less than about 5 Å. The calculated critical distance is much larger than 5 Å. Therefore, the non-radiative energy transfer between Ho^{3+} or Yb^{3+} ions

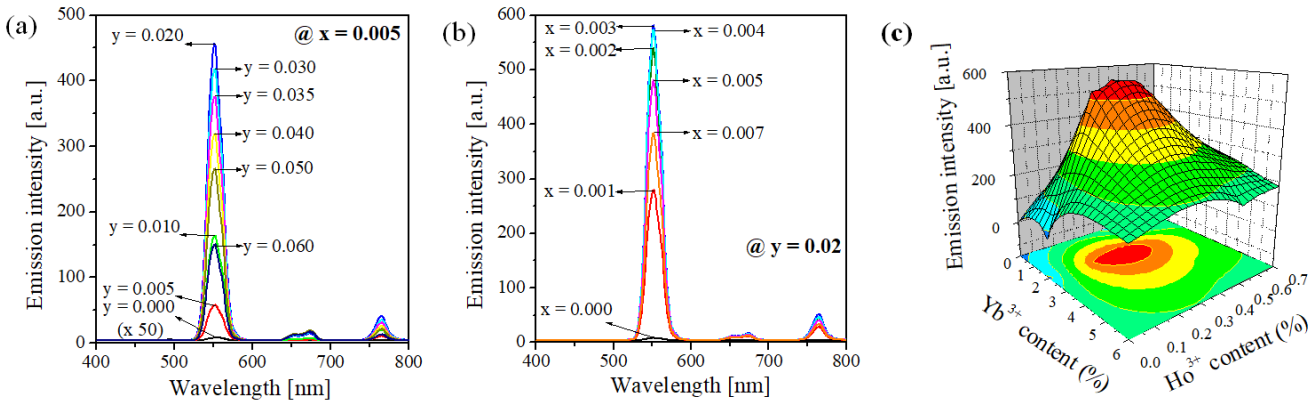

FIG. 4. Concentration effect of Ho^{3+} and Yb^{3+} on the upconversion properties of $Ce_{1-x-y}O_2$:xHo^{3+}/yYb^{3+}: Emission spectra (a and b) and three-dimensional plot of the green emission intensity (c) while changing the amount of Yb^{3+} and Ho^{3+} ions. All samples are calcined at 1200°C.

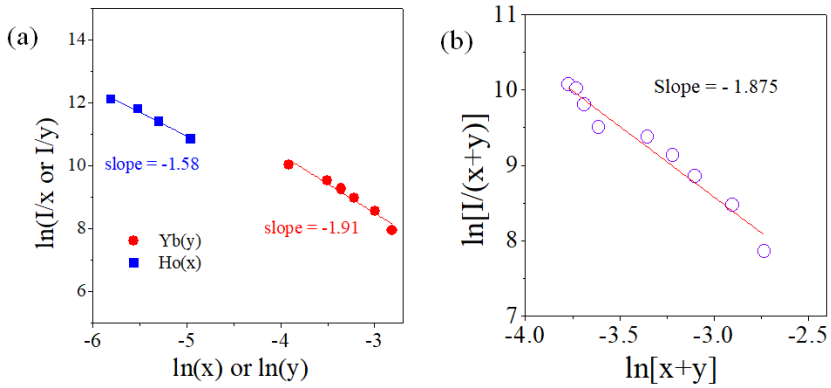

FIG. 5. Linear plots between of (a) ln(I/x or I/y) against ln(x or y) and (b) ln(I/(x+y)) versus ln(x+y) for $Ce_{1-x-y}O_2$:xHo^{3+}/yYb^{3+}.

mainly occurs through the multipolar interaction processes. To elucidate the type of multipolar interaction, the following relation between the emission intensity (I) and the activator concentration (z) can be used [35].

$$\frac{I}{z} = \frac{K}{1+\beta z^{Q/3}}. \quad (2)$$

where K and b are interaction constants. The multipolar character (Q) is 6, 8, and 10 for dipole-dipole, dipole-quadruple and quadruple-quadruple interactions, respectively. The Q value can be estimated from the slope of ln(I/z) vs. ln(z) assuming that $\beta z^{Q/3} \gg 1$. Figure 5(a) shows the fitting of ln(I/z) vs. ln(z) (z = x for Ho^{3+} and z = y for Yb^{3+}). The resulting Q values are 4.74 and 5.73 for Ho^{3+} and Yb^{3+}, respectively. These values are close to 6. In addition, as shown in the inset of Fig. 5(b), the Q value is 5.62 when calculated based on the total dopant concentration, indicating the energy transfer occurs via the dipole-dipole interaction process.

The emission was monitored while changing the IR pumping power in order to investigate the UC mechanism of $CeO_2:Ho^{3+}/Yb^{3+}$. Figure 6(a) shows the emission spectra measured with a current variation of the IR laser for the sample of $CeO_2:Ho_{0.003}/Yb_{0.02}$. The emission progressively increases with the increase of laser current. In UC phosphors, the emission intensity (I) is known to be proportional to P^n, ($I \propto P^n$), where P is the IR pumping power and n presents the photon number for achieving one UC emission. Then, the n value is equal to the slope of ln(I) vs. ln(P) plot. As shown in Fig. 6(b), the n value estimated from the fitting resulting is 1.95, which is close to 2. Therefore, the green emission of $CeO_2:Ho_{0.003}/Yb_{0.02}$ is mainly achieved by the two-photon process. For the $CeO_2:Ho_x/Yb_y$ samples prepared by changing the Ho^{3+} and Yb^{3+} content, the n values were estimated and shown in Figs. 6(c) and 6(d) as a function of the dopant content. For $CeO_2:Ho_{0.005}$, the n value is 1.31. As shown Fig. 6(c), the n value progressively increases up to 2 while increasing the content of Yb^{3+}. At a fixed Yb^{3+} content (y = 0.02), the n values increase monotonically from 1.69 to 2.0 while increasing the Ho^{3+} content from 0.01% to 0.5% (Fig. 6(d)). According to the previous report [36, 37], the UC mechanism can be explained by considering the competition between linear decay and upconversion for the depletion of photons in intermediate states. The intermediate and emission energy levels for the green emission are $^5I_6$ and $^5F_4/^5S_2$ of Ho^{3+}, which are denoted as N_2 and N_4 in Fig.

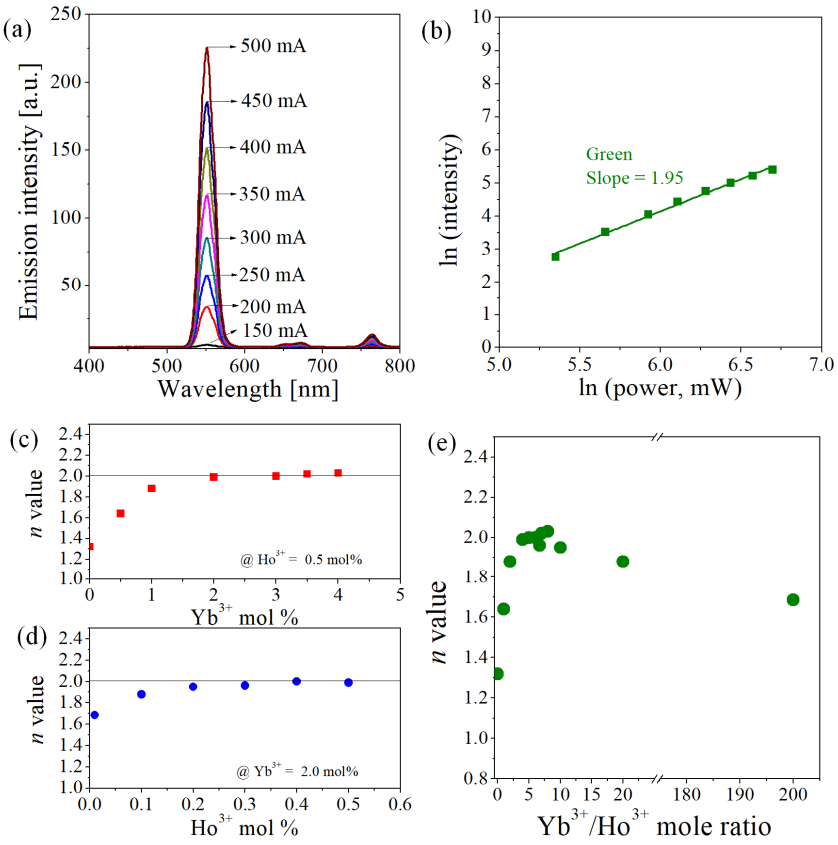

FIG. 6. (a) Upconversion emission spectra at different pumping power and (b) logarithmic dependence of green peak intensity as a function of pumping power for $CeO_2:Ho_x^{3+}/Yb_y^{3+}$ (x=0.003, y=0.02). Changes in the n value as a function of (c) Yb^{3+}mol%, (d) Ho^{3+} mol% and (e) Yb^{3+}/Ho^{3+} mole ratio.

1(b), respectively. When the dominant depletion of photons in the N_2 level is achieved by the linear decay, the emission from the N_4 level is proportional to P^2 ($n = 2$). On the contrary, the UC emission is proportional to P ($n = 1$) when the upconversion is dominant for the photon depletion of the N_2 level. For the sample prepared without Yb^{3+}, the n value is 1.31. Given this, the upconversion dominates the depletion of photons in the intermediate N_2 level when no Yb^{3+} is doped. In the case of codoping Yb^{3+}, the n values progressively increase up to 2.0 with increasing the Yb^{3+} content. The n values remain closely to 2.0 even when the Yb^{3+} concentration is 2.0 mol% or larger. Figure 6(e) shows the n value as a function of the Yb^{3+}/Ho^{3+} mole ratio. The n value rapidly increases until the Yb^{3+}/Ho^{3+} mole ratio becomes about 5 and steadily decreases when the Yb^{3+}/Ho^{3+} mole ratio is larger than about 10. This result indicates that the upconversion mechanism strongly depends on the Yb^{3+}/Ho^{3+} ratio. The energy transfer (ET) from Yb^{3+} to Ho^{3+} can occur in the transition of $^5I_8 \rightarrow {}^5I_6$ ($N_0 \rightarrow N_2$) (GSA) or $^5I_6 \rightarrow {}^5F_4/{}^5S_2$ ($N_2 \rightarrow N_4$) (ESA). If the energy transfer is mainly involved in the $^5I_6 \rightarrow {}^5F_4/{}^5S_2$ transition (ESA process), the photons at the intermediate level ($^5I_6$, N_2) should be depleted by upconversion as the Yb^{3+} content or the Yb^{3+}/Ho^{3+} ratio increases. As a result, the green emission should be proportional to P^1 as the Yb^{3+} content increases. This situation is not in agreement with the experimental data. According to the results shown in Fig. 6(c), even if the Yb^{3+} content increases to larger than 2.0 at%, the n value does not decrease to 2 or less. Therefore, to meet this experimental result, the energy transfer from Yb^{3+} to Ho^{3+} should take place dominantly through the GSA process and the photon depletion at the intermediate level should be mainly caused by the linear decay. However, if the Yb^{3+} content is too high compared with the Ho^{3+} concentration, the energy transfer from Yb^{3+} to Ho^{3+} through the ESA process becomes large and not negligible. That is, the photons at the intermediate energy level (N_2) are competitively consumed by upconversion and linear decay. This is in agreement with the experimental results in which the n value decreases below 2.0 when the Yb^{3+}/Ho^{3+} ratio is greater than 10.

IV. CONCLUSION

$CeO_2:Ho^{3+}/Yb^{3+}$ was prepared synthesized by spray pyrolysis. The resulting $CeO_2:Ho^{3+}/Yb^{3+}$ particles with spherical shape and hollow structure showed intense green emission due to the $^5F_4/{}^5S_2 \rightarrow {}^5I_8$ transition of Ho^{3+} ion and minor peaks in red and NIR under the 980 nm IR irradiation. The Yb^{3+} co-doping clearly made it possible to largely improve the upconversion green emission due to the energy transfer from Yb^{3+} to Ho^{3+}. In terms of achieving the highest emission, the optimal content of Ho^{3+} (x) and Yb^{3+} (y) ions were found to be $x = 0.003$ and $y = 0.02$ in $CeO_2:Ho_x^{3+}/Yb_y^{3+}$. The upconversion emission intensity showed a linear relationship with the crystallite size of CeO_2 and the concentration quenching between the same doping ions was proved to occur mainly via a dipole-dipole interaction process. The green upconversion of $CeO_2:Ho^{3+}/Yb^{3+}$ optimized in terms of the emission intensity was achieved by a typical two-photon process. The energy transfer from Yb^{3+} to Ho^{3+} was concluded to mainly occur in the ground-state adsorption step ($^5I_8 \rightarrow {}^5I_6$) of Ho^{3+} ions unless the Yb^{3+}/Ho^{3+} ratio is greater than 10.

ACKNOWLEDGMENT

This work was supported by the Technology Innovation Program (Advanced Technology Center, ATC) funded by the Ministry of Trade, Industry & Energy, Republic of Korea (Grant no. 10052088).

REFERENCES

1. P. Kumar, K. Nagpal, and B. K. Gupta, "Unclonable security codes designed from multicolor luminescent lanthanide-doped Y_2O_3 nanorods for anticounterfeiting," ACS Appl. Mater. Interfaces **9**, 14301-14308 (2017).
2. K. Y. Jung, J. C. Lee, D. S. Kim, B.-K. Choi, and W.-J. Kang, "Co-doping effect of monovalent alkali metals on optical properties of CeO_2:Eu nanophosphor prepared by spray pyrolysis and application for preparing pearlescent pigments with red emission," J. Lumin. **192**, 1313-1321 (2017).
3. P. Kumar, S. Singh, and B. K. Gupta, "Future prospects of luminescent nanomaterial based security inks: from synthesis to anti-counterfeiting applications," Nanoscale **8**, 14297-14340 (2016).
4. J. Andres, R. D. Hersch, J. E. Moser, and A. S. Chauvin, "A new anti-counterfeiting feature relying on invisible luminescent full color images printed with lanthanide-based inks," Adv. Funct. Mater. **24**, 5029-5036 (2014).
5. Y. Liu, K. Ai, and L. Lu, "Designing lanthanide-doped nanocrystals with both up-and down-conversion luminescence for anti-counterfeiting," Nanoscale **3**, 4804-4810 (2011).
6. G. Chen, H. Qiu, P. N. Prasad, and X. Chen, "Upconversion nanoparticles: design, nanochemistry, and applications in theranostics," Chem. Rev. **114**, 5161-5214 (2014).
7. J. Zhou, Q. Liu, W. Feng, Y. Sun, and F. Li, "Upconversion luminescent materials: advances and applications," Chem. Rev. **115**, 395-465 (2015).
8. H. Suo, C. Guo, Z. Yang, S. Zhou, C. Duan, and M. Yin, "Thermometric and optical heating bi-functional properties of upconversion phosphor $Ba_5Gd_8Zn_4O_{21}:Yb^{3+}/Tm^{3+}$," J. Mater. Chem. C **3**, 7379-7385 (2015).
9. F. Huang, Y. Gao, J. Zhou, J. Xu, and Y. Wang, "Yb^{3+}/Er^{3+} co-doped $CaMoO_4$: a promising green upconversion phosphor for optical temperature sensing," J. Alloys Compd. **639**, 325-329 (2015).
10. S. P. Tiwari, K. Kumar, and V. K. Rai, "Latent fingermarks detection for $La_2O_3:Er^{3+}/Yb^{3+}$ phosphor material in upcon-

version emission mode: A comparative study," J. Appl. Phys. **118**, 183109 (2015).
11. Y. Yang, C. Mi, F. Jiao, X. Su, X. Li, L. Liu, J. Zhang, F. Yu, Y. Liu, and Y. Mai, "A novel multifunctional upconversion phosphor: Yb^{3+}/Er^{3+} codoped La_2S_3," J. Am. Ceram. Soc. **97**, 1769-1775 (2014).
12. G. Boulon, "Why so deep research on Yb^{3+}-doped optical inorganic materials?," J. Alloys Compd. **451**, 1-11 (2008).
13. I. Porosnicu, D. Avram, B. Cojocaru, M. Florea, and C. Tiseanu, "Up-conversion luminescence of Er(Yb)-CeO_2: Status and new results," J. Alloys Compd. **711**, 627-636 (2017).
14. G. Han, M. Wang, D. Li, J. Bai, and G. Diao, "Novel upconversion Er, Yb-CeO_2 hollow spheres as scattering layer materials for efficient dye-sensitized solar cells," Sol. Energy Mater. Sol. Cells **160**, 54-59 (2017).
15. J. Kim, Y. Ryou, G. Hwang, J. Bang, J. Jung, Y. Bang, and D. H. Kim, "Oxychlorination of methane over FeO*x*/CeO_2 catalysts," Korean J. Chem. Eng. **35**, 2185-2190 (2018).
16. J.-H. Park, H. Noh, T.-S. Chang, and C.-H. Shin, "Low-temperature CO oxidation of $Pt/Al_{0.1}Ce_{0.9}O$ *x* catalysts: Effects of supports prepared with different precipitants," Korean J. Chem. Eng. **35**, 645-653 (2018).
17. M. Yada, T. Miyaguchi, D. Watanabe, Y. Hayashi, T. Ayabe, T. Torikai, and T. Watari, "Morphological control and upconversion luminescence of hollow CeO_2 and Er^{3+}-Yb^{3+} codoped CeO_2 particles," CrystEngComm **18**, 8377-8387 (2016).
18. D. Han, Y. Yang, F. Gu, and Z. Wang, "Tuning the morphology and upconversion fluorescence of CeO_2:Er/Yb nano-octahedra," J. Alloys Compd. **656**, 524-529 (2016).
19. Y. Guo, D. Wang, and F. Wang, "Effect of Li^+ ions doping on microstructure and upconversion luminescence of CeO_2:Er^{3+} translucent ceramics," Opt. Mater. **42**, 390-393 (2015).
20. A. Pandey, V. K. Rai, R. Dey, and K. Kumar, "Enriched green upconversion emission in combustion synthesized Y_2O_3:Ho^{3+}-Yb^{3+} phosphor," Mater. Chem. Phys. **139**, 483-488 (2013).
21. Y. Q. Sheng, L. L. Xu, J. Liu, D. Zhai, and Z. G. Zhang, "Improving monochromaticity of upconversion luminescence by codoping Eu^{3+} ions in Y_2O_3:Ho^{3+}, Yb^{3+} nanocrystals," J. Lumin. **130**, 338-341 (2010).
22. A. Pandey and V. K. Rai, "Improved luminescence and temperature sensing performance of Ho^{3+}-Yb^{3+}-Zn^{2+}:Y_2O_3 phosphor," Dalton Trans. **42**, 11005-11011 (2013).
23. P. Du, E.-J. Kim, and J. S. Yu, "Local symmetry distortion-induced enhancement of upconversion luminescence in Gd_2O_3:Ho^{3+}/Yb^{3+}/Zn^{2+} nanoparticles for solid-state lighting and bioimaging," Curr. Appl. Phys. **18**, 310-316 (2018).
24. A. Kumar, S. P. Tiwari, K. Kumar, and V. K. Rai, "Structural and optical properties of thermal decomposition assisted Gd_2O_3:Ho^{3+}/Yb^{3+} upconversion phosphor annealed at different temperatures," Spectrochim. Acta A Mol. Biomol. Spectrosc. **167**, 134-41 (2016).
25. S. Babu, J.-H. Cho, J. M. Dowding, E. Heckert, C. Komanski, S. Das, J. Colon, C. H. Baker, M. Bass, W. T. Self, and S. Seal, "Multicolored redox active upconverter cerium oxide nanoparticle for bio-imaging and therapeutics," Chem. Commun. **46**, 6915-6917 (2010).
26. D. Avram, I. Porosnicu, B. Cojocaru, M. Florea, and C. Tiseanu, "Time-gated down-/up-conversion emission of Ho-CeO_2 and Ho, Yb-CeO_2 nanoparticles," J. Lumin. **179**, 265-271 (2016).
27. S. Mondal, A. T. Derebe, and K. Wang, "Surface functionalized carbon microspheres for the recovery of copper ion from refinery wastewater," Korean J. Chem. Eng. **35**, 147-152 (2018).
28. B. H. Min and K. Y. Jung, Synthesis and luminescence characteristics of fine-sized $Ba_3Si_6O_{12}N_2$:Eu green phosphor through spray pyrolysis using TEOS/Si_3N_4 mixed precursors," RSC Adv. **7**, 44759-44765 (2017).
29. J. Choi, K. S. Yoo, and J. Kim, "Spray pyrolysis synthesis of mesoporous TiO_2 microspheres and their post modification for improved photocatalytic activity," Korean J. Chem. Eng. **35**, 2480-2486 (2018).
30. B. H. Min, J.-H. Choi, and K. Y. Jung, "Improvement of capacitive deionization performance via using a Tiron-grafted TiO_2 nanoparticle layer on porous carbon electrode," Korean J. Chem. Eng. **27**, 272-282 (2018).
31. K. Y. Jung, D. Y. Lee, Y. C. Kang, and H. D. Park, "Improved photoluminescence of $BaMgAl_{10}O_{17}$ blue phosphor prepared by spray pyrolysis," J. Lumin. **105**, 127-133 (2003).
32. J. H. Kang, W. B. Im, D. J. Lee, J. Y. Kim, D. Y. Jeon, Y. C. Kang, and K. Y. Jung, "Correlation of photoluminescence of (Y, Ln)VO_4:Eu^{3+} (Ln = Gd and La) phosphor with their crystal structure," Solid State Commun. **133**, 651-656 (2005).
33. S. H. Lee, D. S. Jung, J. M. Han, H. Y. Koo, and Y. C. Kang, "Fine-sized $Y_3Al_5O_{12}$:Ce phosphor powders prepared by spray pyrolysis from the spray solution with barium fluoride flux," J. Alloys Compd. **477**, 776-779 (2009).
34. G. Blasse, "Energy transfer in oxidic phosphors," Phys. Lett. A **28**, 444-445 (1968).
35. L. Jiang, C. Chang, D. Mao, and C. Feng, "Concentration quenching of Eu^{2+} in $Ca_2MgSi_2O_7$:Eu^{2+} phosphor," Mater. Sci. Eng. B **103**, 271-275 (2003).
36. M. Pollnau, D. R. Gamelin, S. R. Lüthi, and H. U. Güdel, "Power dependence of upconversion luminescence in lanthanide and transition-metal-ion systems," Phys. Rev. B **61**, 3337-3346 (2000).
37. Y. Lei, H. Song, L. Yang, L. Yu, Z. Liu, G. Pan, X. Bai, and L. Fan, "Upconversion luminescence, intensity saturation effect, and thermal effect in Gd_2O_3:Er^{3+},Yb^{3+} nanowires," J. Chem. Phys. **123**, 174710 (2005).